

Ocean biogeochemical fingerprints of fast-sinking tunicate and fish detritus

Jessica Y. Luo¹, Charles A. Stock¹, John P. Dunne¹, Grace Saba², and Lauren Cook²

¹NOAA Geophysical Fluid Dynamics Laboratory

²Rutgers University

November 3, 2023

Abstract

Pelagic tunicates (salps, pyrosomes) and fishes generate jelly-falls and/or fecal pellets that sink roughly 10 times faster than bulk oceanic detritus, but their impacts on biogeochemical cycles in the ocean interior are poorly understood. Using a coupled physical-biogeochemical model, we find that fast-sinking detritus decreased global net primary production and surface export, but increased deep sequestration and transfer efficiency in much of the extratropics and upwelling zones. Fast-sinking detritus generally decreased total suboxic and hypoxic volumes, reducing a “large oxygen minimum zone (OMZ)” bias common in global biogeochemical models. Newly aerobic regions at OMZ edges exhibited reduced transfer efficiencies in contrast with global tendencies. Reductions in water column denitrification resulting from improved OMZs improved simulated nitrate deficits relative to phosphate. The carbon flux to the benthos increased by 11% with fast-sinking detritus from fishes and pelagic tunicates, yet simulated benthic fluxes remained on the lower end of observation-based estimates.

Hosted file

977890_0_art_file_11532752_s3cngw.docx available at <https://authorea.com/users/530580/articles/683931-ocean-biogeochemical-fingerprints-of-fast-sinking-tunicate-and-fish-detritus>

Hosted file

977890_0_supp_11532753_s37f7m.docx available at <https://authorea.com/users/530580/articles/683931-ocean-biogeochemical-fingerprints-of-fast-sinking-tunicate-and-fish-detritus>

1 **Ocean biogeochemical fingerprints of fast-sinking tunicate and fish detritus**

2
3
4 Jessica Y. Luo¹, Charles A. Stock¹, John P. Dunne¹, Grace K. Saba², Lauren Cook²

5
6 ¹NOAA Ocean and Atmospheric Research, Geophysical Fluid Dynamics Laboratory, 201
7 Forrestal Rd, Princeton NJ 08540

8 ²Center for Ocean Observing Leadership, Department of Marine and Coastal Sciences, School of
9 Environmental and Biological Sciences, Rutgers University, New Brunswick, NJ USA

10
11
12 Manuscript correspondence: Jessica.Luo@noaa.gov

13
14
15 *Submitted to Geophysical Research Letters.*

16
17
18 ORCID:

19 JYL: 0000-0002-0032-9370

20 CAS: 0000-0001-9549-8013

21 JPD: 0000-0002-8794-0489

22 GKS: 0000-0002-3874-895X

23
24
25 **Main points:**

- 26
- We incorporated fast-sinking detritus from pelagic tunicates and fishes into a modified version of the ocean biogeochemical model COBALT.
 - The fast-sinking detritus increased carbon sequestration and transfer efficiency to depth, but decreased surface productivity and export.
 - Fast-sinking detritus decreased the size of oxygen minimum zones (OMZs) and water column denitrification, a common model bias.
- 27
28
29
30
31
32

33 **Abstract**

34

35 Pelagic tunicates (salps, pyrosomes) and fishes generate jelly-falls and/or fecal pellets that sink
36 roughly 10 times faster than bulk oceanic detritus, but their impacts on biogeochemical cycles in
37 the ocean interior are poorly understood. Using a coupled physical-biogeochemical model, we
38 find that fast-sinking detritus decreased global net primary production and surface export, but
39 increased deep sequestration and transfer efficiency in much of the extratropics and upwelling
40 zones. Fast-sinking detritus generally decreased total suboxic and hypoxic volumes, reducing a
41 “large oxygen minimum zone (OMZ)” bias common in global biogeochemical models. Newly
42 aerobic regions at OMZ edges exhibited reduced transfer efficiencies in contrast with global
43 tendencies. Reductions in water column denitrification resulting from improved OMZs improved
44 simulated nitrate deficits relative to phosphate. The carbon flux to the benthos increased by 11%
45 with fast-sinking detritus from fishes and pelagic tunicates, yet simulated benthic fluxes
46 remained on the lower end of observation-based estimates.

47

48

49 **Plain Language Summary**

50

51 Marine ecosystems play a critical role in the global carbon cycle through the food web regulation
52 of air-sea carbon fluxes and the transfer of particulate matter from the upper oceans to depth.
53 Recent evidence has suggested that the detritus from fishes and gelatinous zooplankton (GZ),
54 specifically the pelagic tunicates such as salps and pyrosomes, may have a disproportionate
55 impact on the ocean’s biological pump due to them sinking approximately 10x faster than bulk
56 detritus. These fluxes result in increased sequestration of particulate carbon and nutrients into the
57 deep oceans, but their impact on biogeochemical cycles at depth is poorly understood. Here, we
58 investigated the sensitivity of deep ocean carbon, oxygen, and nutrient cycles to fast-sinking
59 detritus from tunicates and fishes. We found that the fast-sinking detritus decreased surface
60 productivity and export, as well as the size of ocean oxygen minimum zones (OMZs). Also, we
61 examined whether observational evidence of seafloor oxygen consumption could support the
62 increased detrital fluxes (and respiration) at depth, and found that even with the increased
63 oxygen consumption, the modeled values were still below the observations. This suggests that
64 these processes could be realistically incorporated into future generations of Earth System
65 Models.

66

67

68 1. Introduction

69

70 In the ocean's biological carbon pump, carbon dioxide (CO₂) is fixed in the surface
71 oceans by algal photosynthesis, and particulate carbon sinks from the surface to depth and
72 regulates the vertical gradient of carbon and nutrients in the ocean (Sarmiento & Gruber, 2006).
73 The strength of this pump is measured by not only how much particulate organic carbon (POC) it
74 exports from the surface oceans (between 4-10 Pg C y⁻¹; DeVries & Weber, 2017; Dunne et al.,
75 2007; Henson et al., 2011), but also how efficiently that exported material sinks to the deep sea
76 (i.e., transfer efficiency or T_{eff}; Francois et al., 2002; Wilson et al., 2022). A range of factors
77 influence T_{eff}: the presence of ballast materials (Armstrong et al., 2002), temperature and
78 oxygen-dependent remineralization (Cram et al., 2018; Marsay et al., 2015), and phytoplankton
79 size structure (Weber et al., 2016). While this understanding is largely based on sediment trap
80 observations (e.g., Armstrong et al., 2002; Martin et al., 1987), a less commonly considered
81 factor is the presence of fast-sinking carcasses (jelly-falls) and/or fecal pellets from gelatinous
82 zooplankton and fishes, which are not well captured in the sediment record.

83 Gelatinous zooplankton (GZ), and in particular, pelagic tunicates (salps, pyrosomes), are
84 notable for their extremely fast-sinking fecal pellets and carcasses, which can exceed 1500 m d⁻¹
85 (Bruland & Silver, 1981; Caron et al., 1989; Lebrato, Mendes, et al., 2013) and result in mass
86 depositions on the seafloor (Henschke et al., 2013; Lebrato, Molinero, et al., 2013; Lebrato &
87 Jones, 2009). Similarly, the fecal pellets of marine fishes can also sink quickly, as the few studies
88 that have measured them show average sinking speeds of 750-1100 m d⁻¹ (Robison & Bailey,
89 1981; Saba & Steinberg, 2012; Staresinic et al., 1983). This is in contrast to marine snow,
90 phytoplankton aggregates, and small crustacean zooplankton (e.g., copepod) fecal pellets that
91 sink at *ca.* 30-300 m d⁻¹ (Turner, 2015). Accordingly, several modeling studies have investigated
92 the impact of fast-sinking GZ-mediated POC on T_{eff} (Clerc et al., 2023; Lebrato et al., 2019; Luo
93 et al., 2020), yet none have investigated the combined effect of GZ and fishes, nor more
94 importantly, the impact of these fast-sinking detritus on biogeochemical cycles in the deep
95 ocean.

96 In addition to direct estimates of detrital flux (sediment traps, Thorium-234 isotopes;
97 Buesseler et al., 2020), the oxygen and macronutrient (e.g., nitrate) concentrations deep in the
98 water column and at the seafloor can also constrain estimates of the biological pump (Andersson
99 et al., 2004; Sulpis et al., 2023). Organic matter remineralization consumes oxygen, but slows
100 significantly in oxygen minimum zones (OMZs) as oxygen is depleted and anaerobic processes,
101 such as denitrification, dominate (Devol & Hartnett, 2001; Van Mooy et al., 2002; Weber &
102 Bianchi, 2020). Unfortunately, the representation of OMZs in coarse-resolution global models
103 has historically been a challenge, with models generally overestimating the extent and
104 misrepresenting the change in OMZs relative to observations (Cabr e et al., 2015; Oschlies et al.,
105 2018; Stramma et al., 2012). While these discrepancies have been attributed in part to weak
106 ventilation and poorly resolved equatorial currents (e.g., Busecke et al., 2019; Duteil et al.,
107 2014), other factors such as the stoichiometry of exported organic matter (Devries & Deutsch,
108 2014; Moreno et al., 2018), and the representation of zooplankton vertical migration (Bianchi et
109 al., 2013) and associated zooplankton-particle interactions (Cavan et al., 2017; Cram et al., 2022)
110 may also influence models' ability to represent observed ocean oxygen patterns. It is unknown,
111 however, whether the inclusion of fast-sinking detritus will exacerbate or alleviate model biases
112 in the OMZs.

113 In this study, we investigate the effects of fast-sinking detritus from tunicates, fishes, and
114 both on biogeochemical cycling using perturbation experiments with a coupled ice-ocean-
115 biogeochemistry model. We assess their impacts on the horizontal and vertical distribution of
116 POC and oxygen in the mesopelagic and deep sea, and quantitatively attribute the fraction of
117 oxygen consumption in the deep sea arising from fast-sinking detritus.

118 119 120 **2. Methods**

121 122 **2.1 Fast-sinking detritus flux**

123 We introduced a new, fast-sinking detritus (1000 m d^{-1}) to the GZ-COBALT model. GZ-
124 COBALT (Luo et al., 2022) incorporated two new (gelatinous) zooplankton groups into the
125 COBALTv2 model (Stock et al., 2020): small and large pelagic tunicates, representing
126 appendicularians and thaliaceans (salps, doliolids, pyrosomes), respectively, with all detritus
127 sinking at the bulk detritus rate (100 m d^{-1}). The other marine ecosystem components
128 (heterotrophic bacteria, small and large phytoplankton, diazotrophs, small, medium, and large
129 zooplankton) remain unchanged. Both pelagic tunicate groups are microphageous generalists,
130 able to consume phytoplankton, bacteria, and heterotrophic nanoflagellates, but preferring
131 smaller sized prey. They are predated upon by mesozooplankton and the unresolved higher
132 trophic-level predators. The higher trophic-level predators, which also predate upon the two
133 mesozooplankton classes, serves as a density-dependent loss for zooplankton (Steele &
134 Henderson, 1992). This provides an estimate of the carbon flux from plankton to epipelagic
135 fishes shown to be consistent with observed cross-ecosystem patterns in fisheries catch (Stock et
136 al., 2017). However, this class excludes mesopelagic fishes, which are not represented in our
137 model, despite potentially comprising significant biomass (Irigoien et al., 2014; Proud et al.,
138 2019). Thus, we will henceforth refer to this group as ‘fish’ and utilize the flux to provide a first-
139 order assessment of epipelagic fish.

140 Detritus in GZ-COBALT is produced from a range of phytoplankton, zooplankton, and
141 fish sources, including phytoplankton aggregation and zooplankton/fish egestion. The fraction of
142 zooplankton egestion going to sinking detritus ranges from 16.7% for microzooplankton to 100%
143 for large mesozooplankton; the rest is partitioned to various dissolved organic matter pools
144 (Stock et al., 2020). Fish and tunicates also generate detritus from 100% of their egestion (fecal
145 pellets), but for fish their egestion fraction is a fixed 35% of ingestion, whereas for tunicates it
146 varies from 20-75% as a function of prey concentration, due to their unique feeding ecology
147 (Harbison et al., 1986; Lombard et al., 2011; Luo et al., 2022). An additional source of tunicate
148 detritus are jelly-falls, which is a mortality that is triggered when ingestion drops below 10% of
149 maximum ingestion rate. Here, only the detritus from large tunicates (thaliaceans) were
150 configured for fast-sinking: 100% of jelly-falls and 75% of egestion. The other 25% of large
151 tunicate egestion is assumed to always sink more slowly (100 m d^{-1}) and represents a
152 combination of pyrosome fecal pellets (Drits et al., 1992) and slow sinking salp and doliolid
153 fecal pellets (Deibel, 1990; Iversen et al., 2017; Patonai et al., 2011; Yoon et al., 2001). For fish,
154 all detritus were fast-sinking (Saba et al., 2021; Saba & Steinberg, 2012; Staresinic et al., 1983).

155 COBALTv2 utilizes seven prognostic tracers to track the various components of detritus:
156 nitrogen (N), phosphorus (P), silica (Si), iron (Fe), lithogenic dust, calcite, and aragonite (Stock
157 et al., 2020). Carbon is associated with detrital N following the Redfield ratio (106:16).
158 COBALTv2 detritus is assumed to sink at 100 m d^{-1} and undergoes temperature- and oxygen-

159 dependent remineralization (Laufkötter et al., 2017). Remineralization is inhibited by the
160 presence of ballast materials such as Si, dust, and calcium carbonate (Armstrong et al., 2002;
161 Klaas & Archer, 2002), as well as above 150 m to account for euphotic zone bacterial
162 colonization (Laufkötter et al., 2017; Mislán et al., 2014). Sinking detritus that reaches the
163 seafloor is subject to remineralization or burial following the parameterization of Dunne et al.
164 (2007), with a ramp down function to reduce burial in nearshore areas. Further dynamics from
165 the simple sediment layer are described in the COBALTv2 documentation (Stock et al., 2020).

166 For fast-sinking detritus, we implemented three new prognostic tracers (for a total of 38)
167 to track fast-sinking N, P, and Fe, which are assumed to sink at 1000 m d^{-1} . This sinking rate
168 represents an approximate median characteristic velocity of salp, pyrosome, and fish fast-sinking
169 detritus (Bruland & Silver, 1981; Caron et al., 1989; Lebrato, Mendes, et al., 2013; Phillips et al.,
170 2009; Saba & Steinberg, 2012; Staresinic et al., 1983; Steinberg et al., 2022). The fast-sinking
171 detritus is also subject to the same temperature- and oxygen-dependent remineralization as the
172 slow sinkers, but not the remineralization inhibiting effects of ballasting nor colonization.

173

174 2.2 Experiments

175 GZ-COBALT with fast POC was run in a global ocean-ice configuration using the
176 Modular Ocean Model 6 (MOM6) and Sea Ice Simulator 2 (SIS2) at a nominal 0.5° horizontal
177 resolution (Adcroft et al., 2019). The model was forced using the 60-year Common Ocean-Ice
178 Reference Experiment II (CORE-II) dataset (Large & Yeager, 2009) and other forcings and
179 initializations as described in Luo et al. (2022). A control and three perturbation experiments
180 were run for five 60-year cycles, or 300 years:

- 181 1) No fast-sinking detritus. All detritus sank at 100 m d^{-1} . (Control simulation)
- 182 2) Only tunicate detritus was fast-sinking.
- 183 3) Only fish detritus was fast-sinking.
- 184 4) Both tunicate and fish detritus were fast-sinking.

185 In the experiments, no other changes to the model were made. Outputs from the last 20 years of
186 the 5th cycle were computed into a climatological mean for analyses.

187

188 2.3 Evaluation

189 For model evaluation, we used particle flux data from 21 observational sites where either
190 free-floating sediment trap or Marine Snow Catcher data were available, compiled by Dinauer et
191 al. (2022), and oxygen and macronutrient concentrations (NO_3 , PO_4) from World Ocean Atlas 18
192 (Garcia et al., 2019a, 2019b). Modeled sediment oxygen utilization rates (OUR) was computed
193 based on POC flux to the bottom, minus burial flux based on Dunne et al. (2007) and sediment
194 denitrification following Middelburg et al. (1996). This was compared with a new global data
195 product of sediment OUR from Jørgensen et al. (2022; hereafter J22), which was constructed
196 using a regression fit to 798 in-situ benthic measurements.

197

198

199 3. Results

200

201 The integration of fast-sinking detritus into GZ-COBALT resulted in an overall decline in
202 net primary production (NPP) and particulate organic carbon (POC) export flux past 100 m
203 relative to the control. NPP decreased 7.8%, 9.5%, and 15%, while export decreased 5.6%, 6.8%,
204 and 11% in the tunicate-only, fish-only, and combined cases, respectively, relative to the GZ-
205 COBALT control (NPP: 52.4 Pg C y⁻¹; export: 6.17 Pg C y⁻¹). Declines in the subtropical gyres
206 were most pronounced as the already limiting surface nutrients redistributed further down in the
207 water column due to the fast-sinking detritus (Fig. 1A). Overall, there was a vertical
208 redistribution of nutrients and detritus, with the tunicate-only and fish-only cases exhibiting
209 similar spatial patterns and magnitudes and the combined case giving values slightly less than the
210 sum of the two others. In the top 100 m, fast-sinking detritus production comprised 6.4%, 8.1%,
211 and 13.9% of the total detritus production in the tunicate-only, fish-only, and combined cases,
212 respectively, but the relative proportion of detritus that was fast-sinking increased with depth.

213 At the sequestration depth, the fast-sinking detritus increased POC flux past 1000 m by
214 19%, 21%, and 37% (to 1.01, 1.02, and 1.15 Pg C y⁻¹ for tunicate-only, fish-only, and combined,
215 respectively; control: 0.84 Pg C y⁻¹), with large increases in much of the extratropics and in
216 upwelling zones (Fig. 1B). A few areas exhibited large declines in POC flux past 1000 m, such
217 as at the northern equatorial Pacific, the northern Indian ocean, the northern Benguela current,
218 and the Canary current. These are all areas where OMZs reduced in size with fast-sinking
219 detritus (Fig. 1B, Fig. 3A) leading to enhanced remineralization rates under newly aerobic
220 conditions. Both transfer efficiency (T_{eff}) and remineralization length scales between 100 m to
221 1000 m exhibited similar patterns as the POC flux past 1000m, albeit significantly muted (Fig.
222 S1A, Fig. 1D). In the subtropical gyres, the POC flux at 1000 m with fast-sinking detritus was
223 slightly lower than the control, but transfer efficiency increased, indicating this pattern was
224 primarily driven by differences in surface production. Overall, remineralization length scales
225 increased globally, except for the aforementioned areas near OMZs.

226 POC flux reaching the seafloor showed broad spatial patterns coherent with those at 100
227 and 1000m. Globally, there were relatively modest enhancements due to the fast-sinking detritus
228 of 5.6%, 6.3%, and 11% (to 1.33, 1.34, and 1.4 Pg C y⁻¹ for tunicate-only, fish-only, and
229 combined, respectively) relative to the control (1.26 Pg C y⁻¹; Fig. 1C). Though, at seafloor
230 depths of 2000 m or deeper, the impact of the fast-sinking detritus was much greater (increases
231 of 36.7%, 39.9%, and 67.2%, respectively, relative to 0.28 Pg C y⁻¹ in the control). Due to faster
232 detritus sinking speeds, the relative contribution of coastal zones (200 m or shallower) to global
233 seafloor fluxes decreased, from 59% in the control case to 52% for both tunicate-only and fish-
234 only, and 47% for tunicates and fish combined. This comes as transfer efficiency to the seafloor
235 (T_{eff_btm}) was globally enhanced, with the largest increases in the eastern equatorial Pacific (Fig.
236 S1B).

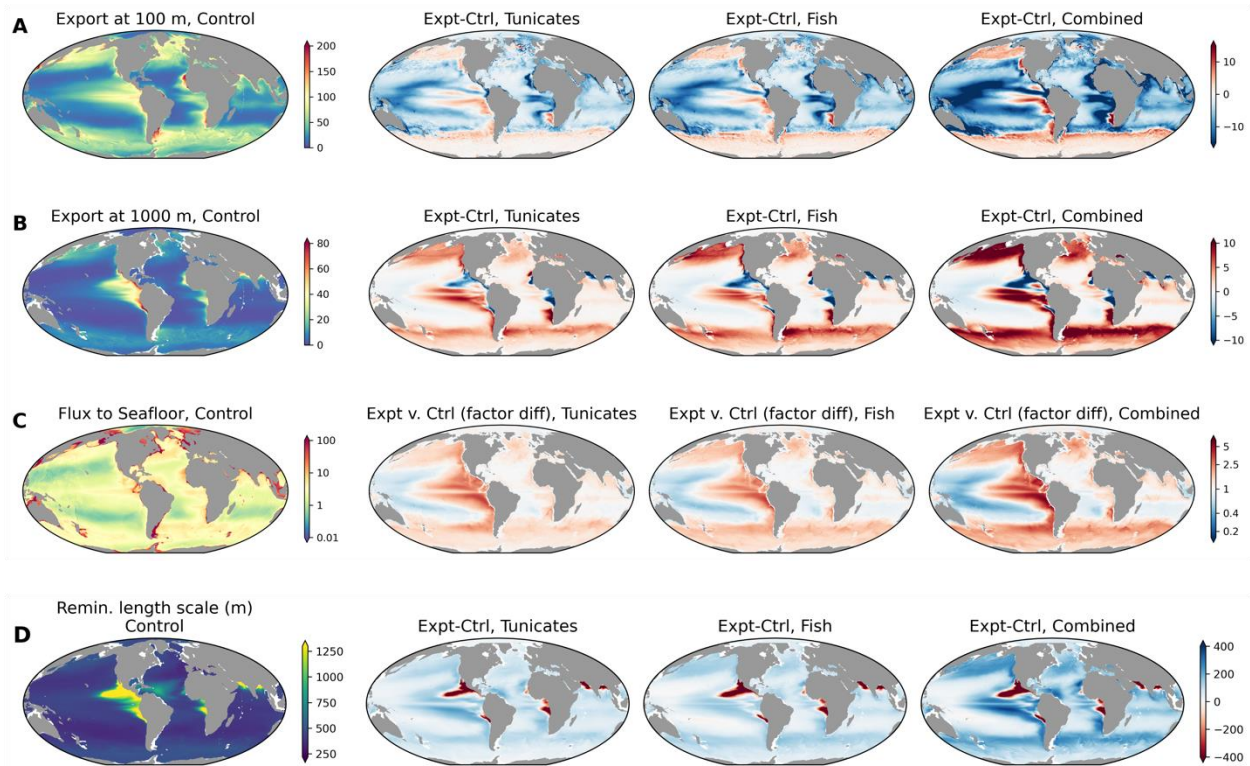
237 A comparison of the POC export flux profiles at 21 sites (Dinauer et al., 2022; Fig. S2)
238 shows that overall, the model simulations with fast-sinking detritus fell within range of the
239 observations (Fig. 2). Given that the COBALT flux attenuation dynamics were tuned to many of
240 the same observations (Laufkötter et al., 2017), it is unsurprising that the observational match, in
241 terms of bias, RMSE, and correlation coefficient, was best in the control simulation at most sites,
242 though in many cases the differences were quite small (Fig. S3; 14/17, or 82%, and 11/21, or
243 52%, of sites had correlation and bias within 5% and 25% of the control, respectively). However,
244 notable exceptions were the MX, VERTEX II, III, and GUAT sites off the western Mexico and

245 Central American coasts, where more fast-sinking detritus significantly improved the model-
246 observational fit. These sites were generally in areas where anaerobic conditions limited export
247 in the control simulation, but not after adding fast-sinking detritus (Fig. 2, S3).

248 An assessment of the biogeochemical impacts of fast-sinking detritus showed the OMZs
249 shrunk and deepened relative to the control, particularly in the combined case (Fig. 3A, Fig. S4-
250 7). An evaluation of the total hypoxic ($O_2 \leq 60 \text{ mmol m}^{-3}$) and suboxic ($O_2 \leq 5 \text{ mmol m}^{-3}$)
251 volume showed that fast-sinking detritus slowed down the expansion of low oxygen zones
252 following model initialization to WOA, and thus reduced the overexpression of hypoxia and
253 suboxia common in global models (Fig. 3D-E). Hypoxia expansion was reduced in all fast-
254 sinking detritus cases through *ca.* 200 years, though the tunicate-only case accelerated to the
255 control simulation afterwards. This was not the case for the fish-only or combined simulations,
256 which remained at a lower hypoxic volume than the control. All fast-sinking detritus experiments
257 decreased the total suboxic volume, with the tunicates and fish combined simulation decreasing
258 suboxia by approximately 40% globally (Fig. 3E). Accordingly, other biogeochemical processes
259 that occur under low oxygen conditions (e.g., denitrification) were also reduced. In the eastern
260 equatorial Pacific, the nitrate deficit in the mesopelagic was much reduced relative to the control
261 (Fig. 3B) and more consistent with observations, as can be seen through the N^* field, which is a
262 metric of the excess nitrate over phosphate (Gruber & Sarmiento, 1997). In the abyssal zone
263 ($>3\text{km}$ deep), the high transfer efficiency of fast-sinking detritus increased nitrate and decreased
264 oxygen, resulting in modest biases in each. Nonetheless, in a zonal slice of the eastern Pacific
265 following the P18 line, model skill metrics for NO_3 , N^* , and to a lesser degree, O_2 , improved
266 with the addition of fast-sinking detritus (Fig. S4-7).

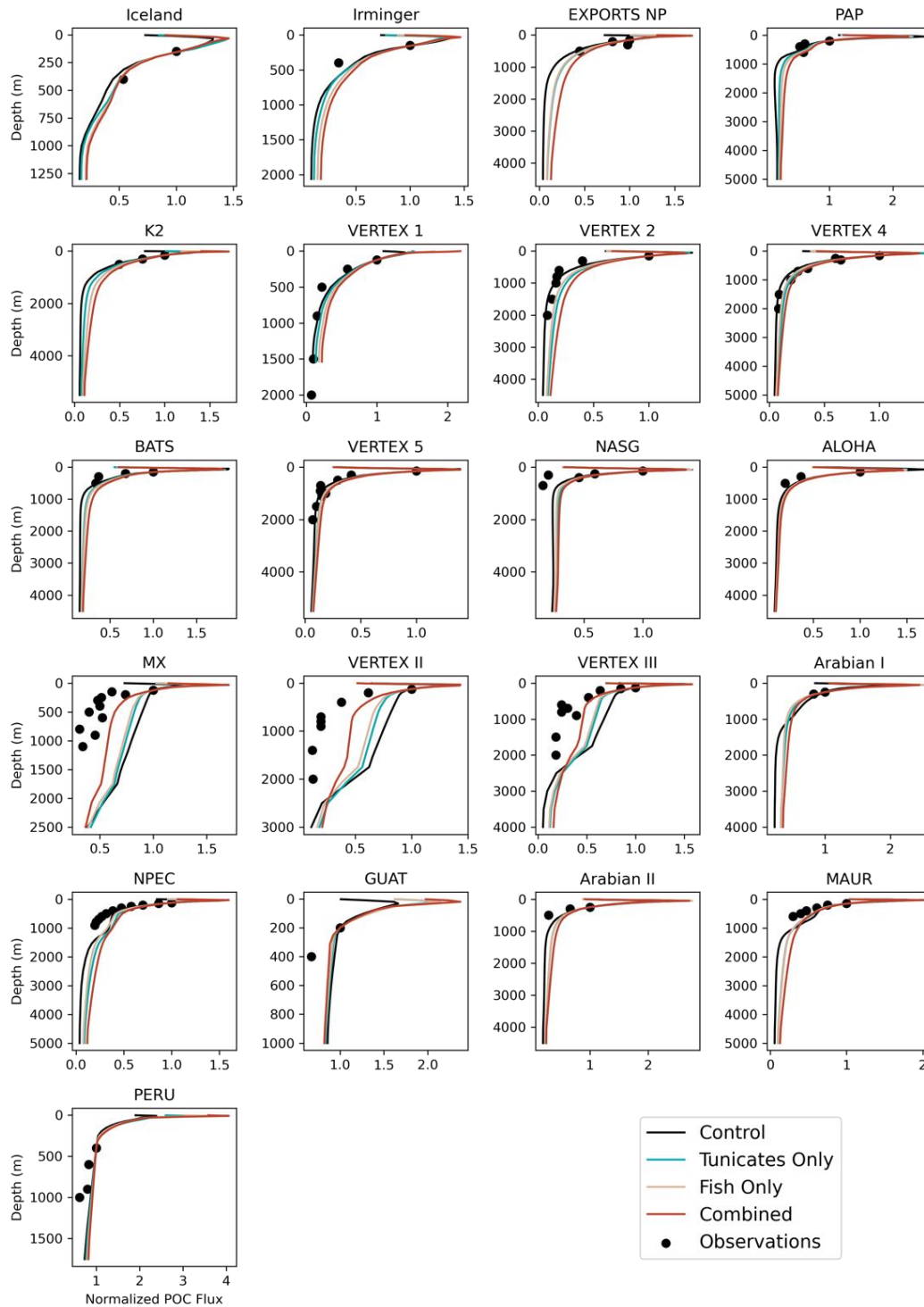
267 The increased supply of POC to the seafloor resulted in increases in benthic oxygen
268 consumption of 6.5%, 7.1%, and 12% (to 110, 111, and 116 $\text{Tmol O}_2 \text{ y}^{-1}$ for tunicate-only, fish-
269 only, and combined) relative to the control (103 $\text{Tmol O}_2 \text{ y}^{-1}$). Even still, values are far lower
270 than the J22 data product, which predicts benthic oxygen utilization rates (OUR) from a linear
271 relationship between NPP and seafloor depth (Fig. 4). This relationship, which was derived from
272 sparse observations, suggests a mean OUR of $1.74 \text{ mmol O}_2 \text{ m}^{-2} \text{ d}^{-1}$, which totals approximately
273 $225 \text{ Tmol O}_2 \text{ y}^{-1}$ globally (given a seafloor area of $3.54\text{E}14 \text{ m}^2$). While J22 did not publish a total
274 range, an estimated range (roughly derived from their 95% CIs) is $\sim 120\text{-}430 \text{ Tmol O}_2 \text{ y}^{-1}$
275 globally. In the combined case, the modeled OUR in the extratropics and upwelling zones
276 approaches the J22 mean, but values in the subtropics from all models were still significantly
277 lower. However, the simulated global OUR in the fast-sinking detritus cases does approach the
278 J22 lower range.

279
280
281
282



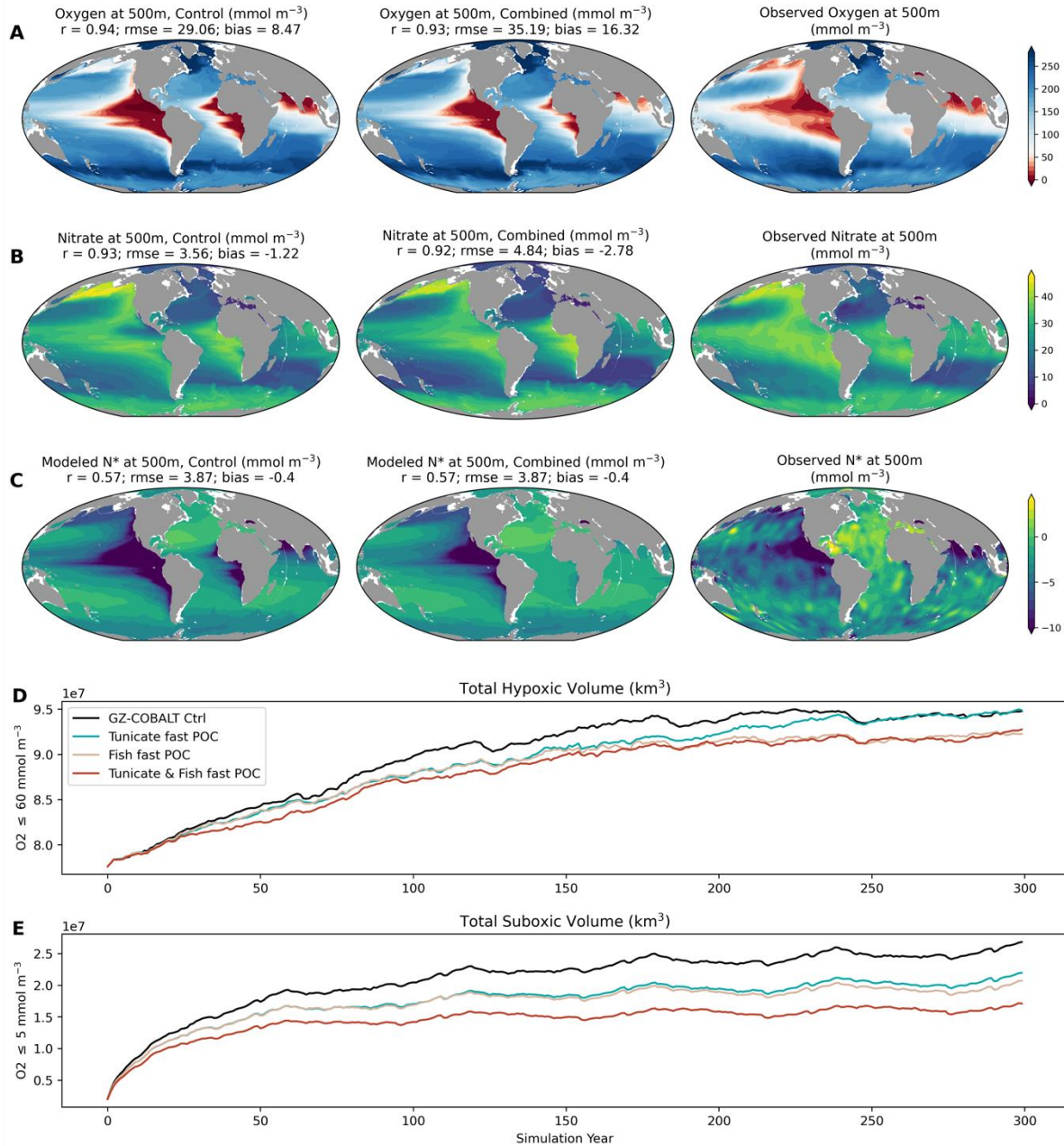
283
 284
 285
 286
 287
 288
 289
 290
 291
 292
 293
 294
 295
 296

Figure 1. Detrital carbon fluxes and remineralization. (A) Particulate organic carbon (POC) export at 100 m ($\text{mg C m}^{-2} \text{d}^{-1}$), showing (left) raw values from the GZ-COBALT control (center to right) the differences between the control and experiments. (B) Same as (A) but at 1000 m. (C) Same as (A) but at the seafloor; note the non-linear colorbars and the use of factor differences. (D) Average remineralization length scale between 100-1000 m, calculated as $r = (1000-100) / \ln(\text{export}_{100}/\text{export}_{1000})$, where export_n refers to the POC export flux at n depth. Colorbars are restricted for display purposes. In the Eastern Tropical North Pacific (ETNP) between $12\text{-}18^\circ \text{N}$ and $92\text{-}112^\circ \text{W}$, the remineralization length scales were 2240 m, 1748 m, 1611 m, and 1416 m for the control, tunicates only, fish only, and combined experiments, respectively. These are associated with transfer efficiencies of 65%, 59%, 57%, and 52%, respectively.

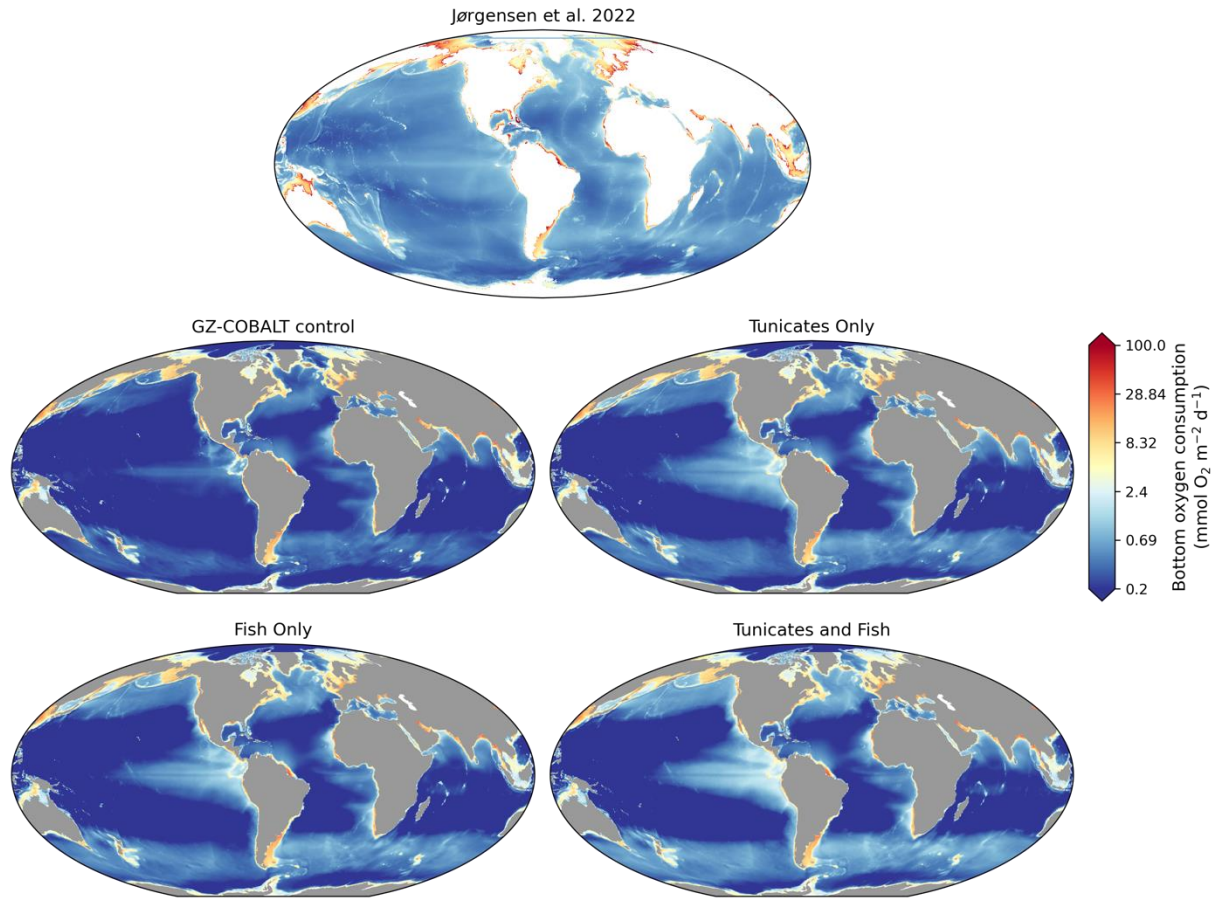


297
 298
 299
 300
 301
 302
 303

Figure 2. Normalized POC export flux at 22 sites (see Fig. S2), comparing the GZ-COBALT control and the three fast-sinking POC simulations with a set of compiled observations of POC flux profiles from either free-drifting sediment traps or with Marine Snow Catchers (Dinauer et al., 2022). Given the seasonal difference in POC flux profiles, model results from only the season, or a 3-month period, in which the observations were obtained were plotted. Comparison statistics are given in Fig. S3.



304
 305 **Figure 3. Ocean biogeochemical impacts of fast-sinking detritus.** Comparisons of (A) oxygen
 306 concentrations ($\text{mmol O}_2 \text{ m}^{-3}$), (B) nitrate concentrations ($\text{mmol NO}_3 \text{ m}^{-3}$), and (C) N^* ($\text{NO}_3 -$
 307 $16 \cdot \text{PO}_4$; mmol m^{-3}) at 500 m depth between the GZ-COBALT control, the tunicates and fish
 308 combined case, and observations from the World Ocean Atlas (WOA). Total (D) hypoxic ($\text{O}_2 \leq$
 309 60 mmol m^{-3}) and (E) suboxic ($\text{O}_2 \leq 5 \text{ mmol m}^{-3}$) ocean volume (in km^3) by simulation year,
 310 shown for the GZ-COBALT control and all three fast-sinking detritus cases. Note that
 311 simulations were initialized from WOA, so the size of the departure from the initial condition in
 312 panels (D) and (E) is proportional to the model bias.
 313



314
315
316
317
318
319

Figure 4. Benthic oxygen utilization. Comparisons between the Jørgensen et al. (2022) observational product (top) and simulated oxygen consumption at the ocean bottom in the GZ-COBALT control and three experimental cases (tunicate-only, fish only, and tunicates and fish combined).

320 4. Discussion

321

322 We used a coupled ocean physical-biogeochemical model to assess the biogeochemical
323 fingerprints of fast-sinking detritus from both pelagic tunicates (e.g., salps, pyrosomes) and
324 fishes in a series of perturbation experiments. The different fast-sinking detritus cases showed
325 that the tunicates-only and fish-only cases were roughly similar in magnitude and spatial extent,
326 with the latter slightly higher along the coasts and in the high productivity regions than the
327 former, consistent with the large scale contrast between tunicates and mesozooplankton in Luo et
328 al. (2022).

329 Overall, addition of fast-sinking detritus decreased global NPP from 52 to 44-48 Pg C y⁻¹,
330 due to the redistribution of ocean nutrients (N, P) from the upper ocean to depth. Accordingly,
331 POC export at 100 m also declined (from 6.2 to 5.5-5.8 Pg C y⁻¹; Fig. 1A), despite increases in
332 the export ratio. While these declines yielded values still within their range of uncertainty (Carr
333 et al., 2006; Dunne et al., 2007; Field et al., 1998), our results highlight that the processes of
334 generating additional and/or fast-sinking ocean detritus reduces euphotic zone productivity, at
335 least on multi-centennial timescales. Compared to a model that adjusted for the surface impacts
336 of some fast-sinking detritus (e.g., Clerc et al., 2023), our results show a much greater decline in
337 surface export flux. This suggests that recalibration of the bulk POC remineralization scheme
338 (Laufkötter et al., 2017) may be necessary to integrate the full spectrum of sinking detritus into
339 an Earth System Model (ESM).

340 Accordingly, model skill in representing normalized export fluxes from observations
341 (Dinauer et al., 2022) were slightly degraded, consistent with modifying a component of a tuned
342 model (Laufkötter et al., 2017). Still, there were notable areas in which normalized export fluxes
343 with fast-sinking detritus were a better match for observations than the control, primarily within
344 eastern boundary currents and in OMZs (Fig. 2, S3). This arises due to the interactive effect of
345 fast-sinking detritus on oxygen and remineralization rates. The total remineralization occurring
346 within a given water volume within the mesopelagic decreases due to fast-sinking detritus, and
347 oxygen increases accordingly (Fig. 3). This results in less anaerobic and more aerobic
348 remineralization. Since aerobic remineralization rates are faster, the remineralization length
349 scales are decreased (Fig. 1D). In COBALT, temperature- and oxygen-dependent aerobic
350 remineralization occurs until oxygen reaches a minimum, 0.8 μmol kg⁻¹, below which anaerobic
351 remineralization occurs at 1/10 the aerobic rate (Laufkötter et al., 2017; Stock et al., 2020). This
352 results in a threshold effect and remineralization length scales within OMZs to be up to 10 times
353 longer than in oxygenated waters (Fig. 1D). In the control simulation, the average mesopelagic
354 remineralization length scale in the Eastern Tropical North Pacific (ETNP) was 2240 m,
355 compared to 1416 m in the fish and tunicates combined case. While there is evidence of long
356 remineralization length scales and high transfer efficiencies in the ETNP, the observations
357 instead support remineralization length scales between 800-1650 m (Devol & Hartnett, 2001;
358 Van Mooy et al., 2002), favoring the simulations with fast-sinking detritus (Fig. 2).

359 Biases in the modeled OMZs have often been attributed to sluggish ventilation and
360 under-resolved equatorial currents in coarse-resolution models (Busecke et al., 2019; Duteil et
361 al., 2014; Getzlaff & Dietze, 2013). So far, the evidence regarding zooplankton-mediated effects
362 on OMZs have indicated that they increase OMZ volume, both through diel vertical migration to
363 the upper margins of the OMZs (Bianchi et al., 2013) and via zooplankton-mediated particle
364 disaggregation (Cram et al., 2022). We acknowledge that there are still significant uncertainties
365 in representing the contribution of fast-sinking detritus from tunicates and fish, such as

366 proportion of detritus that is fast-sinking in both groups (c.f., Iversen et al., 2017) and mineral
367 ballasting in fecal pellets, which is included for the slow-sinking but not fast-sinking detritus in
368 this current formulation. Additionally, we omitted representation of fish carcasses, which may be
369 non-negligible in high productivity areas (Drazen et al., 2012; Higgs et al., 2014), as well as
370 mesopelagic fishes, where there is still substantial uncertainty regarding both overall biomass
371 and metabolic rates governing their contribution to the biological pump (Davison et al., 2013;
372 Irigoien et al., 2014; McMonagle et al., 2023; Proud et al., 2019). Still, the reduction of OMZ
373 volume and associated biases implies an additional, biological mechanism via fast-sinking
374 tunicate and fish detritus for improving OMZ simulation in ocean biogeochemical models.

375 The reduced expansion of OMZs in the fast-sinking detritus cases was most pronounced
376 in the suboxic ($<5 \text{ mmol O}_2 \text{ m}^{-3}$) rather than hypoxic ($<60 \text{ mmol O}_2 \text{ m}^{-3}$) waters (Fig. 3). This is
377 likely due to the shifting of the OMZs deeper due to abyssal respiration (Fig. S4-7). Accordingly,
378 water column denitrification, the reduction of oxidized nitrogen (here, NO_3) to N_2 under low
379 oxygen conditions, also declined, resulting in improvements in negative NO_3 biases between
380 500-2000 m (Fig. S4-7). The modeled oxygen patterns are qualitatively consistent with a recent
381 study by Bianchi et al. (2021), which suggests that fish POC comprise a substantive fraction of
382 oxygen utilization below 1000 m. However, in our simulations, fish POC production comprises
383 $0.56\text{-}0.73 \text{ Pg C y}^{-1}$, significantly less than the 1.5 and 3.0 Pg C y^{-1} as suggested by Saba et al.,
384 (2021) and Bianchi et al. (2021), respectively. Further, contrary to the suggestion that present
385 day ocean deoxygenation (Schmidtko et al., 2017) may be partially masked by declines in fish
386 populations relative to the preindustrial ocean (Bianchi et al., 2021), our results indicate that in a
387 world with significant declines in fish populations, fish detritus would instead be redistributed to
388 be mediated by mesozooplankton instead, which would sink at the slower, “bulk” rate and
389 redistribute nutrients higher in the water column. This would result in an expansion of OMZs, as
390 remineralization would be shifted towards the surface rather than the mesopelagic to abyssal
391 ocean. It is unclear how tunicate populations are likely to respond in the case of significant fish
392 population declines, but as they primarily compete with microzooplankton rather than
393 mesozooplankton (Luo et al., 2022; Stukel et al., 2021), it is unlikely that fast-sinking tunicate
394 detritus could compensate for decreases in fish detritus.

395 A key difficulty in constraining deep-sea biogeochemical fluxes is the lack of
396 observational data; however, sedimentary oxygen utilization may be used as an independent,
397 large-scale biogeochemical constraint, as the seafloor serves as the terminal sediment trap
398 (Andersson et al., 2004; Dunne et al., 2007; Middelburg, 2019). Past estimates have suggested a
399 large-scale concurrence between organic matter respiration as estimated from water column
400 sediment traps vs. sedimentary oxygen utilization rates (OUR), particularly in the open ocean
401 (Dunne et al., 2007; Jahnke, 1996), but it was not clear *a priori* whether such observations would
402 support increased fluxes to the bottom from fast-sinking detritus. Our results show that recent
403 seafloor OUR observations (Jørgensen et al., 2022; J22) support increased organic matter fluxes
404 from fast-sinking detritus relative to our control simulation. Indeed, even with the highest $T_{\text{eff_btm}}$,
405 modeled seafloor OUR was a factor of 2 lower than J22, though likely within uncertainty
406 bounds. Reasons for this discrepancy (see also Andersson et al., 2004; Sulpis et al., 2023) could
407 include biases in both the observations (uneven sampling and bias towards coasts and high
408 productivity areas) and the models (coastal productivity in a coarse-scale model is biased low
409 despite broad skill in simulating NPP; Stock et al., 2014). The large-scale benthic flux patterns
410 between oligotrophic gyres and high latitudes as seen in J22 are better reproduced in the fast-
411 sinking detritus case, but fluxes in subtropical regions remain low. These differences highlight a

412 broader need to reconcile pelagic POC export fluxes with benthic sedimentary demands in
413 ESMs, particularly with increasing focus on coastal zones, blue carbon, and other climate
414 mitigation strategies, where sedimentary dynamics may be increasingly important to resolve.
415
416
417

418 **Acknowledgements**

419 We thank Xiao Liu and Fei Da for their suggestions and comments through an internal review,
420 which improved a previous version of this manuscript. JYL acknowledges support from the
421 NOAA Marine Ecosystem Tipping Points Initiative. We declare no conflicts of interest with
422 respect to the results of this paper.

423

424 **Open Research**

425 All model outputs necessary to reproduce the results in this manuscript are available at Zenodo at
426 <https://doi.org/10.5281/zenodo.8431830>. Fortran code for the model code modifications are at
427 https://github.com/jessluo/ocean_BGC/tree/gz_COBALT, and the analysis codes are available at
428 https://github.com/jessluo/gz_COBALT_fastPOC_analysis.

429

430

431 **References**

- 432
- 433 Adcroft, A., Anderson, W., Balaji, V., Blanton, C., Bushuk, M., Dufour, C. O., et al. (2019). The
 434 GFDL Global Ocean and Sea Ice Model OM4.0: Model Description and Simulation
 435 Features. *Journal of Advances in Modeling Earth Systems*, *11*(10), 3167–3211.
 436 <https://doi.org/10.1029/2019MS001726>
- 437 Andersson, J. H., Wijnsman, J. W. M., Herman, P. M. J., Middelburg, J. J., Soetaert, K., & Heip,
 438 C. (2004). Respiration patterns in the deep ocean. *Geophysical Research Letters*, *31*(3),
 439 L03304. <https://doi.org/10.1029/2003GL018756>
- 440 Armstrong, R. A., Lee, C., Hedges, J. I., Honjo, S., & Wakeham, S. G. (2002). A new,
 441 mechanistic model for organic carbon fluxes in the ocean based on the quantitative
 442 association of POC with ballast minerals. *Deep-Sea Research Part II: Topical Studies in*
 443 *Oceanography*. [https://doi.org/10.1016/S0967-0645\(01\)00101-1](https://doi.org/10.1016/S0967-0645(01)00101-1)
- 444 Bianchi, D., Galbraith, E. D., Carozza, D. A., Mislan, K. A. S., & Stock, C. A. (2013).
 445 Intensification of open-ocean oxygen depletion by vertically migrating animals. *Nature*
 446 *Geoscience*, *6*(7), 545–548. <https://doi.org/10.1038/ngeo1837>
- 447 Bianchi, D., Carozza, D. A., Galbraith, E. D., Guiet, J., & DeVries, T. (2021). Estimating global
 448 biomass and biogeochemical cycling of marine fish with and without fishing. *Science*
 449 *Advances*, *7*(41), eabd7554. <https://doi.org/10.1126/sciadv.abd7554>
- 450 Bruland, K. W., & Silver, M. W. (1981). Sinking rates of fecal pellets from gelatinous
 451 zooplankton (salps, pteropods, doliolids). *Marine Biology*, *63*(3), 295–300.
- 452 Buesseler, K. O., Boyd, P. W., Black, E. E., & Siegel, D. A. (2020). Metrics that matter for
 453 assessing the ocean biological carbon pump. *Proceedings of the National Academy of*
 454 *Sciences*, *117*(18), 9679–9687. <https://doi.org/10.1073/pnas.1918114117>
- 455 Busecke, J. J. M., Resplandy, L., & Dunne, J. P. (2019). The Equatorial Undercurrent and the
 456 Oxygen Minimum Zone in the Pacific. *Geophysical Research Letters*, *46*(12), 6716–
 457 6725. <https://doi.org/10.1029/2019GL082692>
- 458 Cabré, A., Marinov, I., Bernardello, R., & Bianchi, D. (2015). Oxygen minimum zones in the
 459 tropical Pacific across CMIP5 models: mean state differences and climate change trends.
 460 *Biogeosciences*, *12*(18), 5429–5454. <https://doi.org/10.5194/bg-12-5429-2015>
- 461 Caron, D. a., Madin, L. P., & Cole, J. J. (1989). Composition and degradation of salp fecal
 462 pellets: Implications for vertical flux in oceanic environments. *Journal of Marine*
 463 *Research*, *47*, 829–850. <https://doi.org/10.1357/002224089785076118>
- 464 Carr, M. E., Friedrichs, M. A. M., Schmeltz, M., Noguchi Aita, M., Antoine, D., Arrigo, K. R., et
 465 al. (2006). A comparison of global estimates of marine primary production from ocean
 466 color. *Deep-Sea Research Part II: Topical Studies in Oceanography*.
 467 <https://doi.org/10.1016/j.dsr2.2006.01.028>
- 468 Cavan, E. L., Trimmer, M., Shelley, F., & Sanders, R. (2017). Remineralization of particulate
 469 organic carbon in an ocean oxygen minimum zone. *Nature Communications*, *8*(1), 14847.
 470 <https://doi.org/10.1038/ncomms14847>
- 471 Clerc, C., Bopp, L., Benedetti, F., Vogt, M., & Aumont, O. (2023). Including filter-feeding
 472 gelatinous macrozooplankton in a global marine biogeochemical model: model–data
 473 comparison and impact on the ocean carbon cycle. *Biogeosciences*, *20*(4), 869–895.
 474 <https://doi.org/10.5194/bg-20-869-2023>
- 475 Cram, J. A., Weber, T., Leung, S. W., McDonnell, A. M. P., Liang, J., & Deutsch, C. (2018).
 476 The Role of Particle Size, Ballast, Temperature, and Oxygen in the Sinking Flux to the

477 Deep Sea. *Global Biogeochemical Cycles*, 32(5), 858–876.
478 <https://doi.org/10.1029/2017GB005710>

479 Cram, J. A., Fuchsman, C. A., Duffy, M. E., Pretty, J. L., Lekanoff, R. M., Neibauer, J. A., et al.
480 (2022). Slow Particle Remineralization, Rather Than Suppressed Disaggregation, Drives
481 Efficient Flux Transfer Through the Eastern Tropical North Pacific Oxygen Deficient
482 Zone. *Global Biogeochemical Cycles*, 36(1). <https://doi.org/10.1029/2021GB007080>

483 Davison, P. C., Checkley, D. M., Koslow, J. A., & Barlow, J. (2013). Carbon export mediated by
484 mesopelagic fishes in the northeast Pacific Ocean. *Progress in Oceanography*, 116, 14–
485 30. <https://doi.org/10.1016/j.pocean.2013.05.013>

486 Deibel, D. (1990). Still-water sinking velocity of fecal material from the pelagic tunicate
487 *Doliioletta gegenbauri*. *Marine Ecology Progress Series*, 62, 55–60.
488 <https://doi.org/10.3354/meps062055>

489 Devol, A. H., & Hartnett, H. E. (2001). Role of the oxygen-deficient zone in transfer of organic
490 carbon to the deep ocean. *Limnology and Oceanography*, 46(7), 1684–1690.
491 <https://doi.org/10.4319/lo.2001.46.7.1684>

492 Devries, T., & Deutsch, C. (2014). Large-scale variations in the stoichiometry of marine organic
493 matter respiration. *Nature Geoscience*, 7(12), 890–894. <https://doi.org/10.1038/ngeo2300>

494 DeVries, T., & Weber, T. (2017). The export and fate of organic matter in the ocean: New
495 constraints from combining satellite and oceanographic tracer observations. *Global*
496 *Biogeochemical Cycles*. <https://doi.org/10.1002/2016GB005551>

497 Dinauer, A., Laufkötter, C., Doney, S. C., & Joos, F. (2022). What Controls the Large-Scale
498 Efficiency of Carbon Transfer Through the Ocean’s Mesopelagic Zone? Insights From a
499 New, Mechanistic Model (MSPACMAM). *Global Biogeochemical Cycles*, 36(10).
500 <https://doi.org/10.1029/2021GB007131>

501 Drazen, J. C., Bailey, D. M., Ruhl, H. A., & Smith, K. L. (2012). The Role of Carrion Supply in
502 the Abundance of Deep-Water Fish off California. *PLoS ONE*, 7(11), e49332.
503 <https://doi.org/10.1371/journal.pone.0049332>

504 Drits, A. V., Arashkevich, E. G., & Semenova, T. N. (1992). *Pyrosoma atlanticum* (Tunicata,
505 Thaliacea): grazing impact on phytoplankton standing stock and role in organic carbon
506 flux. *Journal of Plankton Research*, 14(6), 799–809.
507 <https://doi.org/10.1093/plankt/14.6.799>

508 Dunne, J. P., Sarmiento, J. L., & Gnanadesikan, A. (2007). A synthesis of global particle export
509 from the surface ocean and cycling through the ocean interior and on the seafloor. *Global*
510 *Biogeochemical Cycles*, 21(4). <https://doi.org/10.1029/2006GB002907>

511 Duteil, O., Schwarzkopf, F. U., Böning, C. W., & Oschlies, A. (2014). Major role of the
512 equatorial current system in setting oxygen levels in the eastern tropical Atlantic Ocean:
513 A high-resolution model study. *Geophysical Research Letters*, 41(6), 2033–2040.
514 <https://doi.org/10.1002/2013GL058888>

515 Field, C. B., Behrenfeld, M. J., Randerson, J. T., & Falkowski, P. (1998). Primary production of
516 the biosphere: Integrating terrestrial and oceanic components. *Science*.
517 <https://doi.org/10.1126/science.281.5374.237>

518 Francois, R., Honjo, S., Krishfield, R., & Manganini, S. (2002). Factors controlling the flux of
519 organic carbon to the bathypelagic zone of the ocean. *Global Biogeochemical Cycles*.
520 <https://doi.org/10.1029/2001gb001722>

521 Garcia, H. E., Weathers, K. W., Paver, C. R., Smolyar, I. V., Boyer, T. P., Locarnini, R. A., et al.
522 (2019a). *World Ocean Atlas 2018. Vol. 4: Dissolved Inorganic Nutrients (phosphate,*
523 *nitrate and nitrate+nitrite, silicate)*.

524 Garcia, H. E., Weathers, K. W., Paver, C. R., Smolyar, I. V., Boyer, T. P., Locarnini, R. A., et al.
525 (2019b). *World Ocean Atlas 2018, Volume 3: Dissolved Oxygen, Apparent Oxygen*
526 *Utilization, and Dissolved Oxygen Saturation*.

527 Getzlaff, J., & Dietze, H. (2013). Effects of increased isopycnal diffusivity mimicking the
528 unresolved equatorial intermediate current system in an earth system climate model:
529 MIMICKING THE EICS. *Geophysical Research Letters*, 40(10), 2166–2170.
530 <https://doi.org/10.1002/grl.50419>

531 Gruber, N., & Sarmiento, J. L. (1997). Global patterns of marine nitrogen fixation and
532 denitrification. *Global Biogeochemical Cycles*, 11(2), 235–266.
533 <https://doi.org/10.1029/97GB00077>

534 Harbison, G. R., McAlister, V. L., & Gilmer, R. W. (1986). The Response of the Salp, *Pegea*
535 *confoederata*, to High Levels of Particulate Material: Starvation in the Midst of Plenty.
536 *Limnology and Oceanography*, 31(2), 371–382.

537 Henschke, N., Bowden, D. A., Everett, J. D., Holmes, S. P., Kloser, R. J., Lee, R. W., & Suthers,
538 I. M. (2013). Salp-falls in the Tasman Sea: a major food input to deep-sea benthos.
539 *Marine Ecology Progress Series*, 491, 165–175. <https://doi.org/10.3354/meps10450>

540 Henson, S. A., Sanders, R., Madsen, E., Morris, P. J., Le Moigne, F., & Quartly, G. D. (2011). A
541 reduced estimate of the strength of the ocean’s biological carbon pump. *Geophysical*
542 *Research Letters*, 38(4). <https://doi.org/10.1029/2011GL046735>

543 Higgs, N. D., Gates, A. R., & Jones, D. O. B. (2014). Fish Food in the Deep Sea: Revisiting the
544 Role of Large Food-Falls. *PLoS ONE*, 9(5), e96016.
545 <https://doi.org/10.1371/journal.pone.0096016>

546 Irigoien, X., Klevjer, T. A., Røstad, A., Martinez, U., Boyra, G., Acuña, J. L., et al. (2014).
547 Large mesopelagic fishes biomass and trophic efficiency in the open ocean. *Nature*
548 *Communications*, 5(1), 3271. <https://doi.org/10.1038/ncomms4271>

549 Iversen, M. H., Pakhomov, E. A., Hunt, B. P. V., van der Jagt, H., Wolf-Gladrow, D., & Klaas,
550 C. (2017). Sinkers or floaters? Contribution from salp pellets to the export flux during a
551 large bloom event in the Southern Ocean. *Deep-Sea Research Part II: Topical Studies in*
552 *Oceanography*, 138(December 2016), 116–125.
553 <https://doi.org/10.1016/j.dsr2.2016.12.004>

554 Jahnke, R. A. (1996). The global ocean flux of particulate organic carbon: Areal distribution and
555 magnitude. *Global Biogeochemical Cycles*, 10(1), 71–88.
556 <https://doi.org/10.1029/95GB03525>

557 Jørgensen, B. B., Wenzhöfer, F., Egger, M., & Glud, R. N. (2022). Sediment oxygen
558 consumption: Role in the global marine carbon cycle. *Earth-Science Reviews*, 228,
559 103987. <https://doi.org/10.1016/j.earscirev.2022.103987>

560 Klaas, C., & Archer, D. E. (2002). Association of sinking organic matter with various types of
561 mineral ballast in the deep sea: Implications for the rain ratio. *Global Biogeochemical*
562 *Cycles*, 16(4), 63-1-63–14. <https://doi.org/10.1029/2001GB001765>

563 Large, W. G., & Yeager, S. G. (2009). The global climatology of an interannually varying air -
564 Sea flux data set. *Climate Dynamics*. <https://doi.org/10.1007/s00382-008-0441-3>

565 Laufkötter, C., John, J. G., Stock, C. A., & Dunne, J. P. (2017). Temperature and oxygen
566 dependence of the remineralization of organic matter. *Global Biogeochemical Cycles*,
567 31(7), 1038–1050. <https://doi.org/10.1002/2017GB005643>

568 Lebrato, M., & Jones, D. O. B. (2009). Mass deposition event of *Pyrosoma atlanticum* carcasses
569 off Ivory Coast (West Africa). *Limnology and Oceanography*, 54(4), 1197–1209.
570 <https://doi.org/10.4319/lo.2009.54.4.1197>

571 Lebrato, M., Mendes, P. D., Steinberg, D. K., Cartes, J. E., Jones, B. M., Birsa, L. M., et al.
572 (2013). Jelly biomass sinking speed reveals a fast carbon export mechanism. *Limnology*
573 *and Oceanography*, 58(3), 1113–1122. <https://doi.org/10.4319/lo.2013.58.3.1113>

574 Lebrato, M., Molinero, J. C., Cartes, J. E., Lloris, D., Melin, F., & Beni-Casadella, L. (2013).
575 Sinking Jelly-Carbon Unveils Potential Environmental Variability along a Continental
576 Margin. *PLoS ONE*, 8(12), e82070. doi:10.1371/journal.pone.0082070.
577 <https://doi.org/10.1371/journal.pone.0082070>

578 Lebrato, M., Pahlow, M., Frost, J. R., Küter, M., Mendes, P. D. J., Molinero, J. C., & Oschlies,
579 A. (2019). Sinking of Gelatinous Zooplankton Biomass Increases Deep Carbon Transfer
580 Efficiency Globally. *Global Biogeochemical Cycles*, 33.
581 <https://doi.org/10.1029/2019GB006265>

582 Lombard, F., Selander, E., & Kiørboe, T. (2011). Active prey rejection in the filter-feeding
583 appendicularian *Oikopleura dioica*. *Limnology and Oceanography*, 56(4), 1504–1512.
584 <https://doi.org/10.4319/lo.2011.56.4.1504>

585 Luo, J. Y., Condon, R. H., Stock, C. A., Duarte, C. M., Lucas, C. H., Pitt, K. A., & Cowen, R. K.
586 (2020). Gelatinous zooplankton-mediated carbon flows in the global oceans: A data-
587 driven modeling study. *Global Biogeochemical Cycles*.
588 <https://doi.org/10.1029/2020GB006704>

589 Luo, J. Y., Stock, C. A., Henschke, N., Dunne, J. P., & O'Brien, T. D. (2022). Global ecological
590 and biogeochemical impacts of pelagic tunicates. *Progress in Oceanography*, 205,
591 102822. <https://doi.org/10.1016/j.pocean.2022.102822>

592 Marsay, C. M., Sanders, R. J., Henson, S. A., Pabortsava, K., Achterberg, E. P., & Lampitt, R. S.
593 (2015). Attenuation of sinking particulate organic carbon flux through the mesopelagic
594 ocean. *Proceedings of the National Academy of Sciences*, 112(4), 1089–1094.
595 <https://doi.org/10.1073/pnas.1415311112>

596 Martin, J. H., Knauer, G. A., Karl, D. M., & Broenkow, W. W. (1987). VERTEX: carbon cycling
597 in the northeast Pacific. *Deep Sea Research Part A. Oceanographic Research Papers*,
598 34(2), 267–285.

599 McMonagle, H., Llopiz, J. K., Hilborn, R., & Essington, T. E. (2023). High uncertainty in fish
600 bioenergetics impedes precision of fish-mediated carbon transport estimates into the
601 ocean's twilight zone. *Progress in Oceanography*, 217, 103078.
602 <https://doi.org/10.1016/j.pocean.2023.103078>

603 Middelburg, J. J. (2019). *Marine Carbon Biogeochemistry: A Primer for Earth System Scientists*.
604 Cham: Springer International Publishing. <https://doi.org/10.1007/978-3-030-10822-9>

605 Middelburg, J. J., Soetaert, K., Herman, P. M. J., & Heip, C. H. R. (1996). Denitrification in
606 marine sediments: A model study. *Global Biogeochemical Cycles*, 10(4), 661–673.
607 <https://doi.org/10.1029/96GB02562>

608 Mislan, K. A. S., Stock, C. A., Dunne, J. P., & Sarmiento, J. L. (2014). Group behavior among
609 model bacteria influences particulate carbon remineralization depths. *Journal of Marine*
610 *Research*, 72(3), 183–218. <https://doi.org/10.1357/002224014814901985>

611 Moreno, A. R., Hagstrom, G. I., Primeau, F. W., Levin, S. A., & Martiny, A. C. (2018). Marine
612 phytoplankton stoichiometry mediates nonlinear interactions between nutrient supply,
613 temperature, and atmospheric CO₂; *Biogeosciences*, *15*(9),
614 2761–2779. <https://doi.org/10.5194/bg-15-2761-2018>

615 Oschlies, A., Brandt, P., Stramma, L., & Schmidtko, S. (2018). Drivers and mechanisms of
616 ocean deoxygenation. *Nature Geoscience*, *11*(7), 467–473.
617 <https://doi.org/10.1038/s41561-018-0152-2>

618 Patonai, K., El-Shaffey, H., & Paffenhofer, G.-A. (2011). Sinking velocities of fecal pellets of
619 doliolids and calanoid copepods. *Journal of Plankton Research*, *33*(7), 1146–1150.
620 <https://doi.org/10.1093/plankt/fbr011>

621 Phillips, B., Kremer, P., & Madin, L. P. (2009). Defecation by *Salpa thompsoni* and its
622 contribution to vertical flux in the Southern Ocean. *Marine Biology*, *156*(3), 455–467.
623 <https://doi.org/10.1007/s00227-008-1099-4>

624 Proud, R., Handegard, N. O., Kloser, R. J., Cox, M. J., & Brierley, A. S. (2019). From
625 siphonophores to deep scattering layers: uncertainty ranges for the estimation of global
626 mesopelagic fish biomass. *ICES Journal of Marine Science*, *76*(3), 718–733.
627 <https://doi.org/10.1093/icesjms/fsy037>

628 Robison, B. H., & Bailey, T. G. (1981). Sinking rates and dissolution of midwater fish fecal
629 matter. *Marine Biology*, *65*(2), 135–142. <https://doi.org/10.1007/BF00397077>

630 Saba, G. K., & Steinberg, D. K. (2012). Abundance, Composition and Sinking Rates of Fish
631 Fecal Pellets in the Santa Barbara Channel. *Scientific Reports*, *2*(1), 716.
632 <https://doi.org/10.1038/srep00716>

633 Saba, G. K., Burd, A. B., Dunne, J. P., Hernández-León, S., Martin, A. H., Rose, K. A., et al.
634 (2021). Toward a better understanding of fish-based contribution to ocean carbon flux.
635 *Limnology and Oceanography*, *66*(5), 1639–1664. <https://doi.org/10.1002/lno.11709>

636 Sarmiento, J. L., & Gruber, N. (2006). *Ocean biogeochemical dynamics*. Princeton: Princeton
637 University Press.

638 Schmidtko, S., Stramma, L., & Visbeck, M. (2017). Decline in global oceanic oxygen content
639 during the past five decades. *Nature*, *542*(7641), 335–339.
640 <https://doi.org/10.1038/nature21399>

641 Staresinic, N., Farrington, J., Gagosian, R. B., Clifford, C. H., & Hulbert, E. M. (1983).
642 Downward Transport of Particulate Matter in the Peru Coastal Upwelling: Role of the
643 Anchoveta, *Engraulis Ringens*. In E. Suess & J. Thiede (Eds.), *Coastal Upwelling Its
644 Sediment Record: Part A: Responses of the Sedimentary Regime to Present Coastal
645 Upwelling* (pp. 225–240). Boston, MA: Springer US. [https://doi.org/10.1007/978-1-4615-
646 6651-9_12](https://doi.org/10.1007/978-1-4615-6651-9_12)

647 Steele, J. H., & Henderson, E. W. (1992). The role of predation in plankton models. *Journal of
648 Plankton Research*, *14*(1), 157–172. <https://doi.org/10.1093/plankt/14.1.157>

649 Steinberg, D. K., Stamieszkin, K., Maas, A. E., Durkin, C. A., Passow, U., Estapa, M. L., et al.
650 (2022). The outsized role of salps in carbon export in the subarctic Northeast Pacific
651 Ocean. *Global Biogeochemical Cycles*. <https://doi.org/10.1029/2022GB007523>

652 Stock, C. A., Dunne, J. P., & John, J. G. (2014). Global-scale carbon and energy flows through
653 the marine planktonic food web: An analysis with a coupled physical–biological model.
654 *Progress in Oceanography*, *120*, 1–28. <http://dx.doi.org/10.1016/j.pocean.2013.07.001>

655 Stock, C. A., John, J. G., Rykaczewski, R. R., Asch, R. G., Cheung, W. W. L., Dunne, J. P., et al.
656 (2017). Reconciling fisheries catch and ocean productivity. *Proceedings of the National*
657 *Academy of Sciences*, 201610238. <https://doi.org/10.1073/pnas.1610238114>
658 Stock, C. A., Dunne, J. P., Fan, S., Ginoux, P., John, J., Krasting, J. P., et al. (2020). Ocean
659 Biogeochemistry in GFDL's Earth System Model 4.1 and Its Response to Increasing
660 Atmospheric CO₂. *Journal of Advances in Modeling Earth Systems*, 12(10).
661 <https://doi.org/10.1029/2019MS002043>
662 Stramma, L., Oschlies, A., & Schmidtko, S. (2012). Mismatch between observed and modeled
663 trends in dissolved upper-ocean oxygen over the last 50 yr. *Biogeosciences*, 9(10), 4045–
664 4057. <https://doi.org/10.5194/bg-9-4045-2012>
665 Stukel, M. R., Décima, M., Selph, K. E., & Gutiérrez-Rodríguez, A. (2021). Size-specific
666 grazing and competitive interactions between large salps and protistan grazers.
667 *Limnology and Oceanography*, 66(6), 2521–2534. <https://doi.org/10.1002/lno.11770>
668 Sulpis, O., Trossman, D. S., Holzer, M., Jeansson, E., Lauvset, S. K., & Middelburg, J. J. (2023).
669 Respiration Patterns in the Dark Ocean. *Global Biogeochemical Cycles*, 37(8),
670 e2023GB007747. <https://doi.org/10.1029/2023GB007747>
671 Turner, J. T. (2015). Zooplankton fecal pellets, marine snow, phytodetritus and the ocean's
672 biological pump. *Progress in Oceanography*, 130, 205–248.
673 <https://doi.org/10.1016/j.pocean.2014.08.005>
674 Van Mooy, B. A. S., Keil, R. G., & Devol, A. H. (2002). Impact of suboxia on sinking
675 particulate organic carbon: Enhanced carbon flux and preferential degradation of amino
676 acids via denitrification. *Geochimica et Cosmochimica Acta*, 66(3), 457–465.
677 [https://doi.org/10.1016/S0016-7037\(01\)00787-6](https://doi.org/10.1016/S0016-7037(01)00787-6)
678 Weber, T., & Bianchi, D. (2020). Efficient Particle Transfer to Depth in Oxygen Minimum
679 Zones of the Pacific and Indian Oceans. *Frontiers in Earth Science*, 8, 376.
680 <https://doi.org/10.3389/feart.2020.00376>
681 Weber, T., Cram, J. A., Leung, S. W., DeVries, T., & Deutsch, C. (2016). Deep ocean nutrients
682 imply large latitudinal variation in particle transfer efficiency. *Proceedings of the*
683 *National Academy of Sciences*, 113(31), 8606–8611.
684 <https://doi.org/10.1073/pnas.1604414113>
685 Wilson, J. D., Andrews, O., Katavouta, A., De Melo Viríssimo, F., Death, R. M., Adloff, M., et
686 al. (2022). The biological carbon pump in CMIP6 models: 21st century trends and
687 uncertainties. *Proceedings of the National Academy of Sciences*, 119(29), e2204369119.
688 <https://doi.org/10.1073/pnas.2204369119>
689 Yoon, W., Kim, S., & Han, K. (2001). Morphology and sinking velocities of fecal pellets of
690 copepod, molluscan, euphausiid, and salp taxa in the northeastern tropical Atlantic.
691 *Marine Biology*, 139(5), 923–928. <https://doi.org/10.1007/s002270100630>
692
693
694